J Nanopart Res (2024) 26:26
https://doi.org/10.1007/s11051-024-05934-3

RESEARCH PAPER

Physicochemical characterization and biological effect of 3D-nanofibrous alumina scaffolds produced by solution blow spinning

Danyella Carolyna Soares dos Reis · Camila Rodrigues Borges Linhares · Rosiane Maria da Costa Farias · Deborah Santos Gomes · Gelmires de Araújo Neves · Jonas Dantas Batista · Paula Dechichi · Leticia de Souza Castro Filice · Romualdo Rodrigues Menezes · Flaviana Soares Rocha

Received: 23 October 2023 / Accepted: 17 January 2024 / Published online: 29 January 2024

Abstract The objective of this study was to conduct a physicochemical characterization and *in vivo* assessment of the bioactivity of amorphous 3D-nanofibrous alumina scaffolds, manufactured using the Solution Blow Spinning (SBS) technique, for the purpose of bone regeneration. The nanofibers utilized in this research were derived from a solution containing aluminum nitrate, polyvinylpyrrolidone (PVP), ethanol, and distilled water, and were subsequently spun using SBS. The resulting scaffolds underwent calcination at 500 °C. Physicochemical analysis of the scaffolds was carried out, and their biological effects were evaluated in the femurs of Wistar rats. The scaffolds exhibited an amorphous structure consisting of nanofibers with an average diameter of 290 nm. They presented a cotton-wool-like 3D configuration after calcination process. Histomorphometric analysis revealed a significantly higher degree of bone neoformation within the alumina groups compared to the control group during both experimental periods ($p < 0.05$). Additionally, the percentage of remaining alumina graft particles was consistent at 14 and 28 days. In conclusion, the assessed 3D nanofibrous alumina scaffolds facilitated bone deposition and supported the filling of bone defects with new bone tissue.

D. C. S. dos Reis · C. R. B. Linhares
Graduate Program in Integrated Dental Clinic, Faculty of Dentistry, Federal University of Uberlândia, Uberlândia, MG, Brazil

R. M. da Costa Farias · D. S. Gomes · G. de Araújo Neves · R. R. Menezes
Laboratory of Materials Technology (LTM), Federal University of Campina Grande, Campina Grande, PB, Brazil

J. D. Batista
Department of Oral and Maxillofacial Surgery and Implantology, Federal University of Uberlândia, Uberlândia, MG, Brazil

P. Dechichi
Biomedical Science Institute, Federal University of Uberlândia, Uberlândia, MG, Brazil

L. de Souza Castro Filice
Faculty of Medicine, Federal University of Uberlândia, Uberlândia, MG, Brazil

F. S. Rocha (✉)
Dentistry Department, University of Brasília, Brasília, DF, Brazil
e-mail: flaviana.rocha@unb.br

F. S. Rocha
Departamento de Odontologia, Faculdade de Ciências da Saúde, Universidade de Brasília, Campos Universitário Darcy Ribeiro S/N - Asa Norte, Brasília, Distrito Federal, Brasil

Keywords Bone healing · Scaffolds · Alumina · Solution Blow Spinning · Biomedicine · Nanocomposites

Introduction

Tissue engineering faces a crucial hurdle: designing functional materials that foster cell-material interactions and enhance tissue repair. Currently, dense alpha alumina (corundum) finds application in orthopedic prostheses [1] and dental implants [2] due to their biocompatibility, chemical inertness, oxidation resistance, and exceptional mechanical properties [3–6]. Nevertheless, the bioinert nature of dense alumina severely restricts its clinical use, stemming from its lack of active bonding with human bone tissue and the absence of interaction with neighboring cells [7].

The demand for bone scaffolds that facilitate new tissue growth is soaring. Recent years have unveiled the bioactivity of nano-porous amorphous alumina nanofilms, showing high protein adsorption (e.g., fibronectin) and osteoblast proliferation [4, 5, 8–10]. In 1999, the first *in vitro* study spotlighting the influence of nanoscale ceramic grain size on osteoblast adhesion revealed that nanophase alumina exhibited significantly higher osteoblast adhesion compared to conventional micron-sized alumina substrates [11].

Other similar studies demonstrated the ability to impact cellular attachment and mineralization in osteoblasts [4, 12, 13] and mesenchymal stem cells [5, 14] by manipulating the pore size of nanostructured amorphous alumina membranes *in vitro*. Most of these studies tweaked anodization processing parameters [4, 12, 14] to produce amorphous nanostructured alumina into thin membranes [4, 5, 12–14] with promising results.

However, the existing literature still lacks investigations into the production of three-dimensional (3D) amorphous alumina nanofibrous scaffolds possessing both bioactivity potential and customized shapes tailored to specific bone damage scenarios. Additionally, the current trend acknowledges the capability of nanofibrous structures to emulate the extracellular matrix due to their high porosity, substantial surface area, and nanostructured fiber surfaces that promote cell adhesion and proliferation [15–17].

Conversely, Solution Blow Spinning (SBS), a nanofiber fabrication technique devised in the early twenty-first century [18], presents a straightforward and swift solution. This method easily yields 3D nanofibrous structures with ample open porosity and nanostructured fibers, promoting cell infiltration, enhanced adhesion, and proliferation. SBS has been successfully adapted to create ceramic nanofibers [19–21]. A recent development demonstrated SBS's potential for crafting 3D-nanofibrillar scaffolds from bioactive glasses, exhibiting strong osteogenesis capability [22]. Thus, this study aimed to conduct a physicochemical evaluation and *in vivo* assessment of the bioactivity of amorphous 3D-nanofibrous alumina scaffolds produced through the SBS technique for bone regeneration.

Materials and Methods

Materials

Aluminum nitrate nonahydrate (Sigma- Aldrich®, Brazil) and polyvinylpyrrolidone (PVP, Mw ~ 1,300,000 g/mol, amorphous) were employed as the inorganic and organic precursors, respectively, to create hybrid fibers. Ethanol (EtOH, 99.5%, Synth®, Brazil) and distilled water were used as solvents for the preparation of the solutions.

Solutions and scaffold production

Solutions were prepared by dissolving aluminum nitrate nonahydrate (2.206 g) in a 2:1 ethanol/water mixture (10 ml) under vigorous magnetic stirring for 1 h at room temperature. Further, 10wt% of PVP was slowly added to the solution and stirred for 1 h.

The fibers were spun immediately after preparing the precursor solutions using an SBS apparatus. This system, described previously [20], is composed of a compressed air source (with pressure regulator), a syringe pump (to control the injection rate of solutions), a spray assembly consisting of an internal and an external nozzle, and a collector. The final solution was transferred to a syringe and injected with a rate of 6.6 mL/h into the inner channel of the SBS nozzle. Compressed air flowed through the external nozzle. The high velocity air after decompression, when released from the external nozzle, acts as a driving force for the spinning process. The solution pumped through the inner nozzle produces a droplet at the tip of the nozzle, which is stretched by the high-speed air from the outer nozzle and jets of solutions erupt from the tip. These jets dry as they move towards the collector along the working distance, producing fibers. The spinning air pressure was set at 0.34 MPa. Fibers were spun across a tubular furnace (working distance) with a temperature of 60 °C to help solvent evaporation. The fibers were collected on a static collector placed in a chamber at 80 °C. The spinning apparatus and processing parameters is detailed in previous works [20, 22, 23]. The as-spun fibers formed a 3D cotton-wool-like scaffold (nanostructured in the form of fibers), which were then calcined at 500 °C for 2 h.

Physicochemical characterization of the scaffold

X-ray diffraction analysis (XRD) was conducted using the XRD-6000 instrument from Shimadzu, Japan. CuKα radiation ($\lambda = 1.5418$ Å) was employed at 40 kV and 30 mA, operating in fixed time mode with a step size of 0.02°. To assess scaffold morphology, scanning electron microscopy (SEM) and atomic force microscopy (AFM) were employed, utilizing the SSX-550 SEM and SPM 9600 AFM models from Shimadzu, Japan, respectively. Fiber diameter measurements were carried out using the ImageJ software developed by the National Institute of Health, USA, with a minimum of 300 individual fiber diameters recorded.

For determining specific surface area through Brunauer–Emmett–Teller (BET) analysis, and pore size and volume through Barrett-Joyner-Halenda (BJH) analysis, the nitrogen adsorption–desorption isotherm technique was adopted. This analysis was performed using the Autosorb-iQ instrument from Quantachrome, USA. Nitrogen adsorption was executed post degassing at 200 °C for a duration of 2 h.

Zeta potential was measured utilizing the Zetasizer nano ZS90 instrument from Malvern, UK.

Animals

Twenty male Wistar rats (*Rattus norvegicus*) with an average weight of 300 ± 20 g and aged 10 weeks were housed under standard conditions. These conditions included a 12-h light/dark cycle, a temperature of 22 ± 1 °C, and a relative humidity range of 50–60%. The rats had access to food (with the following composition: humidity, crude protein, ethereal extract, mineral, crude fiber, calcium, and phosphorus) and water ad libitum.

Ethical considerations were followed for all experimental procedures involving animals. The protocols were approved by the Committee on the Ethics of Animal Use and Care at the Federal University of Uberlândia, with permit number 088/17. Moreover, all activities were carried out strictly in line with the recommendations outlined in the Guide for the Care and Use of Laboratory Animals published by the National Institutes of Health (NIH Publications No. 8023, revised 1978).

Surgical procedure

Following a week of acclimatization, the animals underwent anesthesia via an intraperitoneal injection containing 100 mg/kg of 10% ketamine and 7 mg/kg of 2% xylazine hydrochloride. After trichotomy and proper antisepsis procedures, bone defects were introduced into both femurs, adhering to the technique outlined by Batista et al. [24].). In brief, with the animal placed in right lateral decubitus, a 2 cm longitudinal incision exposed the outer surface of the right femur. Subsequently, a complete-thickness cortical bone osteotomy, utilizing a round bur under saline irrigation, led to the formation of a 2.3 mm bone defect. In the Control Group, the defects were randomly packed with coagulous, while in the Test Group, 3D-nanofibrous alumina scaffolds were employed. The defects were then categorized into four groups (n = 5) for each designated sacrifice period: Control (14 days), Control (28 days), Alumina (14 days), and Alumina (28 days). The wound was effectively sutured using Nylon 4.0 thread.

Euthanasia and Sample Collection

All animals were euthanized either 14- or 28-days post-surgery through intraperitoneal injection of sodium thiopental and lidocaine. This process was carried out in accordance with the tenets of the Universal Declaration on Animal Welfare. Following euthanasia, cervical dislocation was performed. The diaphysis containing the bone defect was promptly immersed in a PBS-buffered formalin solution (4%, pH 7.4) for 48 h at room temperature. After the fixation process, a thorough wash was administered, and the bone underwent decalcification in a 10% ethylene diamine tetra acetic acid solution (pH 7.2). Finally, the prepared bone samples were embedded in paraffin for further analysis.

Histomorphometry Analysis

Semi-serial sections measuring 5 µm were extracted from the center of the bone defects. These sections were subsequently subjected to Hematoxylin and Eosin (HE) staining, as well as Mallory Trichrome (MT) staining. Histological assessments were conducted using an optical microscope (Olympus BX50, Olympus Imaging America Inc., Shinjuku-ku, Tokyo, Japan).

To determine the percentage of newly formed bone and remaining graft particles in relation to the total area of the bone defect, three sections stained with Mallory Trichrome were employed for each defect. This methodology was adopted in line with the approach outlined by Batista et al. (2014) [24]. Essentially, the bone defect, or the region of interest (ROI), was demarcated by four straight lines spanning from the edges of the affected cortical area to the opposite cortical side. The quantification of the newly formed bone and graft particle remnants within this defined region was achieved using the measuring tool within Image J 1.53 (developed by Wayne Rasband, National Institutes of Health, USA).

Statistical Analysis

The data were subjected to analysis using GraphPad Prism (GraphPad Prism® version 5.0 for Windows, San Diego, CA, USA). Initially, the acquired values underwent the Kolmogorov–Smirnov normality test. Subsequently, the parameters were assessed employing unpaired t-tests, and statistical significance was attributed to differences with a p-value of less than 0.05.

Results and discussion

Scaffold production

The current study is the first using the innovative amorphous 3D-nanofibrous alumina scaffolds, constructed in the form of fibers through thermal treatment of SBS scaffolds. This approach seeks to attain a suitable open structure conducive to bone regeneration. The method presented here diverges from the commonly encountered techniques in the literature for fabricating alumina-based biomaterials.

Nanostructured alumina materials are commonly synthesized through anodization processing [4, 12, 14]. While this approach shows promise, it has limitations in creating 3D-scaffolds in the form of nanoscale fibers. Anodized alumina is typically derived from aluminum, which imposes restrictions on the overall volume that can undergo anodization. Consequently, most studies employing this method have focused on nanostructured alumina in the form of thin membranes [4, 5, 12–14]. In contrast, electrospinning (ES) stands as the foremost top-down technique for producing ceramic nanofibers [25–27]. Investigations using this approach have yielded: (1) α-alumina (α-Al2O3) fibers with diameters ranging from 20 to 500 nm post calcination between 900 and 1300ºC [28]; (2) α-Al2O3 fibers with diameters spanning 150 to 500 nm after calcination at 1200 °C [25]; (3) α-Al2O3 fibers with diameters between 100 and 500 nm following firing at 1000 °C [26]; and (4) α-Al2O3 fibers with diameters from 102 to 378 nm after firing at 1200ºC Additionally, ES has been employed for generating γ-phase alumina (γ-Al2O3) fibers, ranging from 114 to 390 nm in diameter after calcination at 800ºC [27]. However, it is crucial to acknowledge that electrospinning comes with the drawbacks of being time-intensive and challenging to assemble fibers into large-scale 3D structures, which in turn results in suboptimal porous architectures [29].

In comparison to the afore-mentioned techniques, Solution Blow Spinning (SBS) holds a distinct appeal due to its ability to tailor the morphological attributes of the resulting scaffolds [18, 22] more precisely, catering to the specific demands of bone repair. This technique also provides a means of effectively controlling material properties, such as pore size and membrane thickness, in a consistent and reproducible manner [18, 29]. Notably, the fibers are swiftly processed and collected, forming diverse architectures including cotton-wool-like structures. This inherent characteristic of SBS enables the potential creation of 3D-nano scaffolds, taking the form of fibers with exceptional nanoscale porosity [19, 20]. Hence, SBS emerges as a high-yielding and promising methodology in the realm of developing 3D-nanofibrous systems.

Scaffold characterization

The XRD pattern of the 3D-nanofibrillar alumina scaffolds is presented in Fig. 1. The pattern lacks diffraction reflections, which is indicative of an amorphous material. It is worth noting that anodic alumina (or anodic aluminum oxide, AAO) also features a similar amorphous structure. AAO, known for its biocompatibility, exhibits a microstructure characterized by nanopores that promote the adhesion and proliferation of osteoblasts [30, 31]. Consequently, the manufactured alumina exhibits a structure that holds the potential to support the osteogenesis process.

The scaffolds generated consist of nanofibers with an approximately circular cross-section, alongside a limited occurrence of bead-shaped structures (Fig. 2A-B). These beads can be attributed to instabilities arising during the spinning process, a phenomenon observed in other studies involving the SBS of oxide ceramic nanofibers [19, 21]. Figure 2C presents the distribution of fiber diameters. The fibers possess an average diameter of 287 nm, exhibiting a wide diameter range, with most fibers falling within the 100 to 500 nm interval.

The clinical efficacy of novel ceramic materials predominantly lies on processes happening at the tissue-material interface [32]. When a graft is introduced into a bone defect, regions within distinct particles become encompassed by a blood clot. This clot serves as a source of vital proteins and growth factors, initiating the sequence of events with cell adhesion and culminating in bone repair [32]. Consequently, given that biomaterial surfaces form the initial point of interaction with the host, attributes like roughness, attachment sites, macro morphology like the extracellular matrix (ECM), and surface charge hold paramount significance in orchestrating the subsequent biological cascade that drives bone healing. In an ideal scenario, a bioactive graft material should engage with surrounding cells, favoring bone formation while also ensuring secure biodegradation [7].

Considering these observations, the distinctive features of nanofibrous alumina open up promising avenues for diverse approaches in tissue engineering [12, 33]. Presently, 3D nanofibrous scaffolds have gained attention due to their capability to mimic the extracellular matrix (ECM), thereby enhancing cell adhesion, proliferation, and the growth of new tissues. The produced scaffolds exhibit such a morphology, comprised of non-oriented interwoven fibers with a high porosity of interconnected pores, like a cotton wool.

Recently, several studies have employed Solution Blow Spinning (SBS) to create amorphous γ-Al2O3 and α-Al2O3 microfibers [34, 35] with mean diameters of 4 µm (ranging from 3.0 µm to 5.5 µm) [34] and spanning a range of 1.5 to 47 µm [35]. However, these investigations did not explore nanofiber diameters or achieve 3D cotton-like structures as accomplished in the present study. This novel 3D architecture and nanofibrous attributes of the material

Fig. 1 XRD patterns of the produced 3D-nanofibrous alumina scaffolds

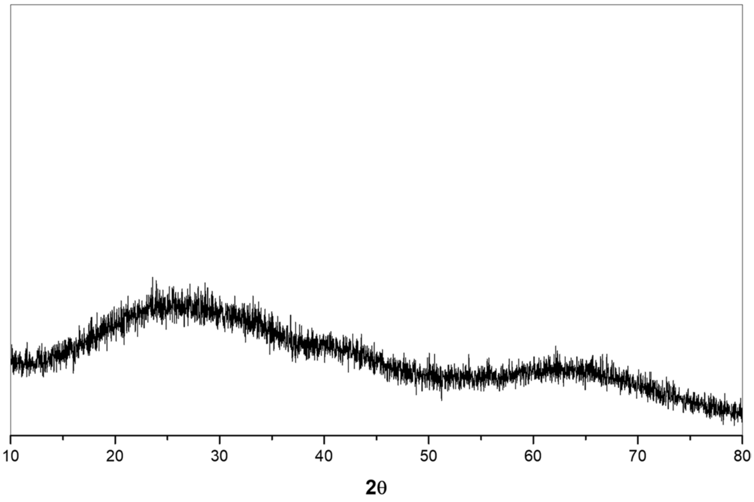

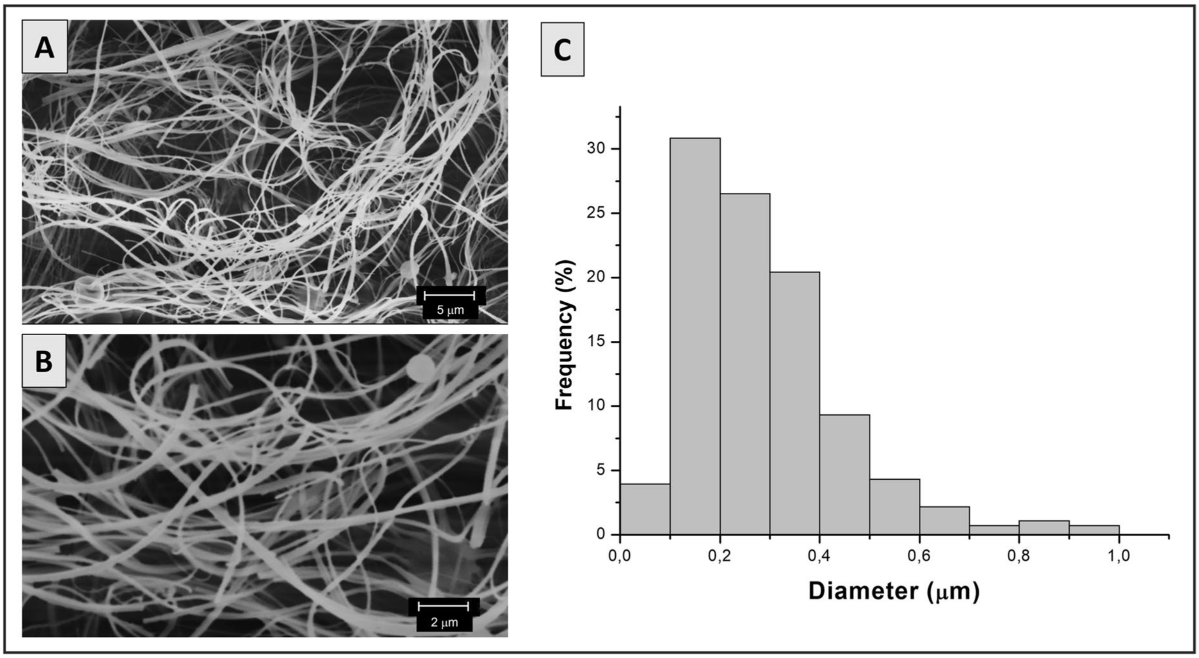

Fig. 2 **A**-**B** Scanning Electron Microscope (SEM) images in different magnification; **C** Graphical representation of fiber diameter distribution for the produced 3d-nanofibrous alumina scaffolds. (Magnification level indicated in the images)

generated in our study are innovative, rendering it suitable for numerous potential applications.

Surface roughness is important for protein attachment, cell spreading and proliferation [36–38]. Figure 3 shows an AFM image of a fiber along with the nano roughness profile in its length. These fibers exhibit an arithmetic mean deviation of roughness (Ra) measuring 5.2 nm, a root mean square deviation of roughness (Rq) at 6.5 nm, and a maximum height of profiles (Rz) at 35.1 nm. These values depict fibers characterized by nano-featured surface topography.

Research has observed that surfaces characterized by nano-featured topography and nano roughness exhibit better efficacy in fostering bone cell adhesion,

Fig. 3 Atomic force microscopy (AFM) images and nano roughness profile along an alumina fiber

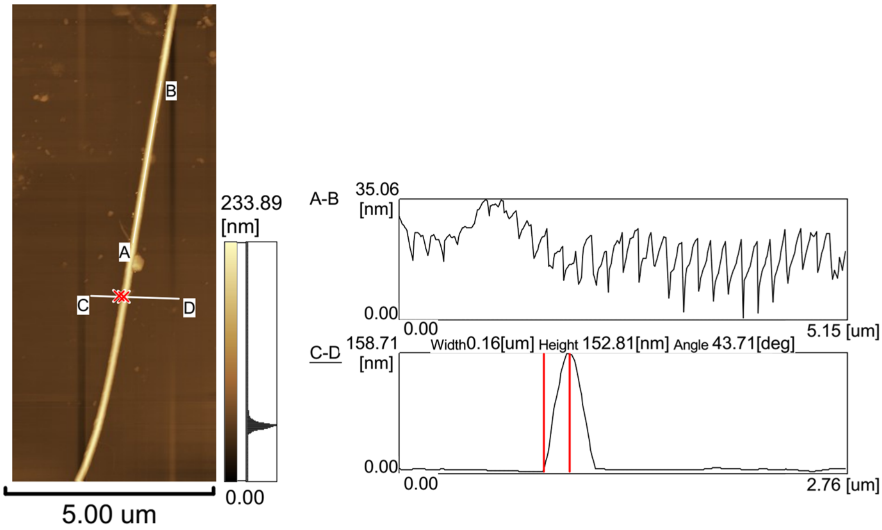

proliferation, and differentiation, when compared to surfaces with coarser topographies (micro or submicron scale roughness) [39, 40]. Nano roughness has the potential to elevate surface hydrophilicity, possibly even transitioning toward super hydrophilic behavior. Additionally, it can enhance the adhesion of peptides and proteins, which in turn encourages cell spreading [36, 41, 42].

Refining the surface of alumina films and supports to a nano scale, encompassing nano roughness and nanometer-sized pores (ranging from 20 to 80 nm), has been shown to enhance the adhesion of osteoblasts and promote the osteogenic differentiation and proliferation of mesenchymal stem cells [5, 10, 36, 42]. Furthermore, studies have indicated that utilizing alumina nanoparticles (ranging from 24 to 167 nm) to generate cell supports introduces a nano roughness to the surface, leading to a 50% improvement in osteoblast adhesion [10, 11, 43].

Figure 4 presents the nitrogen adsorption–desorption isotherm alongside the BJH pore diameter distribution curve. These fibers exhibit a BET surface area measuring 22 m^2/g, a pore volume (BJH) of 0.119 cm^3/g, and a pore size distribution spanning from 2 to 60 nm. Notably, the modes for pore sizes are observed around 2 nm and 6 nm. It's important to note that the observed pore sizes of the fibers are lower than those reported in the literature for alumina surfaces with nano roughness employed for cell adhesion and proliferation, as these typically fall within the range of meso and microporosity (20 to 80 nm).

The produced scaffolds exhibit an interwoven fiber morphology, with the fibers featuring micropores and surface nano roughness. However, these attributes alone aren't solely responsible for robust cell growth; surface charge also plays a pivotal role in ensuring effective cellular adherence. The fibers demonstrate an average zeta potential of + 6.4 mV at a pH of 7.3.

In water, alumina nanoparticles have a positive surface charge ($Al\text{-}OH_2^+$) (at acidic pH, protonation creates a positively charged alumina surfaces) in a wide range of pH, up to the point of zero charge, which range from 7.6 to 9 [39, 44, 45]. At alkaline pH the surface is negative ($Al\text{-}O^-$) due to the amphoteric nature of the Al–OH groups. However, according to Kosmulski [46], the point of zero charge (PZC) of aluminas can range at a larger pH interval, from 6.5 to 10.0. Thus, the zeta potential of + 6.4 mV at a pH of 7.3 obtained is coherent with literature values.

Researchers [39] have observed an isoelectric point (IEP) at a pH of 6.7 for AAO, resulting in a negative charge at physiological pH levels ranging from 7.4 to 8.0. The fibers generated in this study, despite having a similar amorphous structure, exhibit a higher IEP (> 7.3). This discrepancy could be from distinct hydrolysis and/or protonation behaviors

Fig. 4 Nitrogen adsorption–desorption isotherm and insert with BJH pore diameter distribution curve

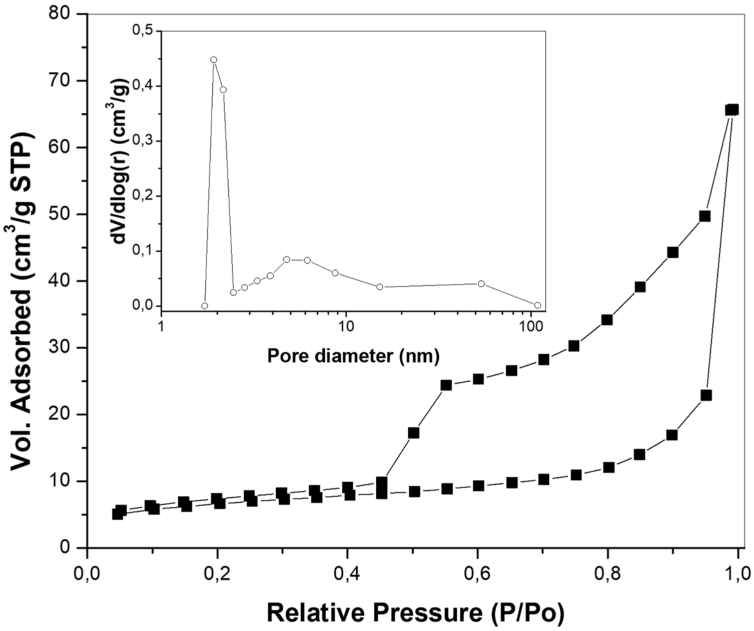

between the produced alumina and AAO. Studies [39, 47] depicted that hydroxyl groups [Al–OH] are formed on the AAO surface when the alumina is immersed in water and that IEP of aluminas varies with surface topology, notably the surface curvature. Small pores (high curvature radius) favour the formation of hydroxyl groups (such as Al_2-OH, Al_3-OH or Al_2-OH_2, with coordination of oxygen to two of three aluminium atoms) with higher affinity to deprotonation [39, 47], which would decrease IEP values.

On the other hand, AAO porous materials have a honeycomb-like structure with cylindrical nanopores, but the N_2 adsorption–desorption graph (Fig. 4) of the produced fibers is a s type IV isotherm with H4 hysteresis loop, which indicates the presence of a mesoporous structure but with slit-type pores [44]. Thus, the difference in surface charge behaviour of the produced material and AAO can be associated with pores morphology and their curvature radius, which generates hydroxyl groups on the surface with different affinity to protonation and consequently different IEP.

The surface charge of the material holds strong influence over the interaction between the scaffold and inorganic and bioorganic constituents present within the cell growth medium. A negative surface is particularly interesting because it facilitates calcium fixation, thereby accelerating apatite nucleation and promoting cell growth. On the other hand, the adsorption of organic compounds is a more complex process, exerting influence over the success of cell adhesion and migration [11, 39].

Initially, researchers presumed that positively charged scaffolds would induce robust cell proliferation. This line of thinking stemmed from the fact that proteins in the extracellular matrix (ECM) bear a negative charge within physiological mediums/pH levels, implying that they would readily adsorb onto the support, consequently augmenting cell adhesion [48]. However, investigations have demonstrated that the adsorption of proteins like osteopontin and fibronectin depends on a multitude of factors beyond the polarity of the support's charge [49, 50]. Additionally, surface charge plays a role in determining the migratory morphology of cells [49, 50], and a charged support enhances adhesion of osteoblast-like cells independently of charge polarity [49]. Thus, the presence of a positive charge on the surface of the generated fibers is important for enhancing cell attachment.

Biological effect—Histological observations and histomorphometry analysis

In the Control Group, bone tissue exhibited a typical morphological appearance, forming trabeculae that enclosed small cavities that partially filled the defect. In the Alumina Group, primary bone tissue predominantly occupied the defect, with large number of osteocytes embedded within the bone matrix, accompanied by numerous remaining graft particles. Areas of secondary bone tissue were infrequent, even after 28 days. Cubic osteoblasts with cytoplasmic basophilia were evident along the bone matrix, indicative of protein synthesis activity. Notably, the remnant graft particles were incorporated into the bone matrix, with signs of remodeling frequently seen (Fig. 5).

Histomorphometric analysis revealed a greater amount of newly formed bone in the Alumina groups in comparison to the Control group during both experimental time periods ($p < 0.05$). Interestingly, the percentage of remnant graft in the Alumina group remained similar at both 14 and 28 days (Fig. 6).

In the present study, 3D-nanofibrous amorphous alumina scaffolds were employed in an animal model to assess their efficacy in promoting bone regeneration. The results revealed greater bone neoformation within the alumina groups as compared to the control group, with a rate of biomaterial degradation like the rate of bone formation. This equilibrium is particularly significant for bone substitutes, as the biomaterial's resorption must not be faster than bone deposition. This dynamic ensures effective filling of the defect with new bone while preserving its original architecture [7]. The progression of bone remodeling was evident in both control and experimental groups, demonstrating the biocompatibility and bioactivity of the tested scaffolds, and their osteoinductive and osteoconductive properties.

These favorable events observed *in vivo* are greatly influenced by material porosity [33, 51, 52] and chemistry [33, 51], and involves recruitment and infiltration of cells from the surrounding bone tissue, as well as vascularization. The penetration of blood vessels is facilitated, in part, by the material's porosity. This is an important issue for oxygen supply, nutrients transport and waste exist from the cells involved in bone repair Additionally, it is well-established in the literature that scaffold pore size and porosity

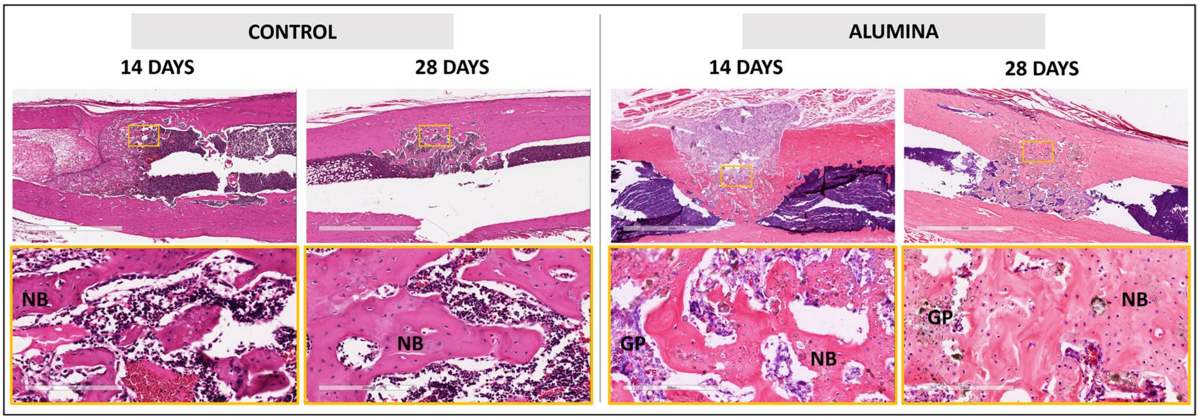

Fig. 5 New bone formation in Control and Alumina Groups. Observe the emergence of new bone in both the Control and Alumina Groups. Notably, new bone growth is observed around the remaining graft particles within the Alumina Group. NB: new bone; GP: graft particles. HE (magnification level indicated in the image)

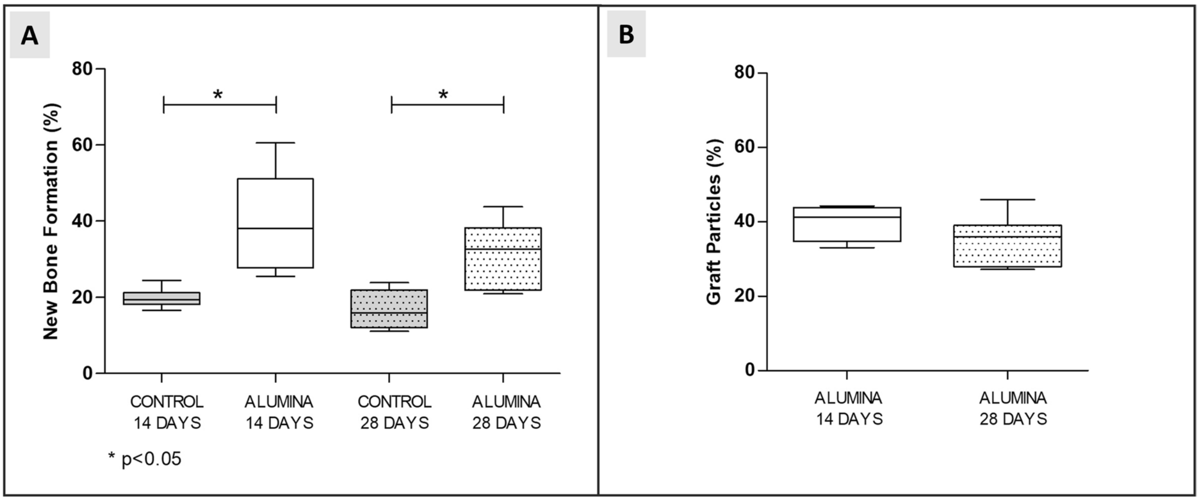

Fig. 6 Histomorphometric Analysis of New Bone Formation (**A**) and Graft Particles (**B**) in Control and Alumina Groups after 14 and 28 Days of Implantation (*$p < 0.05$)

mediates the behavior of mesenchymal cells [5, 53], increasing osteogenic differentiation and proliferation [4, 12]. This is mandatory for the clinical success of biomaterials.

Although the specific behavior of bone cells was not evaluated *in vitro*, the present *in vivo* study effectively demonstrated the successful use of 3D-alumina scaffolds, characterized by pores ranging from 100 to 500 nm, for bone repair and regeneration.

The interaction between cells and the surface of amorphous 3D-nanofibrous alumina scaffolds can also be attributed to their hydrophilicity. It has been documented that nanophase alumina exhibits greater hydrophilicity compared to conventional alumina [11]. Notably, improved adhesion of human osteoblasts are found on the more hydrophilic materials that presented a higher protein adsorption [54]. As a consequence, shortly after the implantation of the scaffold, vital interactions occur between proteins and the surfaces of the biomaterial [55] creating a stable and highly textured nanoscale surface. This environment becomes conducive to bone deposition.

The amorphous or crystalline phases of ceramic scaffolds can influence the osteogenic induction process [51]. Prior *in vitro* investigations have demonstrated the osteoinductive potential of nanostructured amorphous alumina membranes [4]. These findings suggest that the nanofibers produced in this study may elicit similar responses *in vivo*, even with the disparities in spinning techniques and material structures. The alumina utilized in this experiment was subjected to calcination at 500 °C, yielding amorphous 3D-nanofibrous alumina scaffolds, as confirmed through fiber characterization. It's worth noting that amorphous materials tend to degrade more faster than crystalline ones due to the less ordered arrangement of their molecular chains, leading to lower material density [6]. Even so, the reabsorption rate of the tested 3D-alumina scaffolds allowed bone deposition and facilitated effective filling of the bone defect with new bone. This observation underscores the capacity of these scaffolds to harmoniously balance degradation and new bone formation.

Conclusion

The synthesis method employed allowed the creation of controlled, cost-effective, and reproducible cotton-wool-like 3D-nanofibrous alumina scaffolds. These scaffolds displayed amorphous nanofibers, approximately 290 nm in diameter, which promoted bone. These discoveries highlight the necessity for additional exploration in this domain. Further research varying crystallinity of the scaffolds to control the imbalance between degradation and new bone formation and *in vivo* analysis in critical size bone defects are necessary to validate and confirm the results presented here.

Acknowledgements The authors would like to thank CNPq (grant nos. 420004/2018-1 and 309771/2021-8), FAPEMIG (grant no. 03063-16) and FAPESQ (Bidding Term Pronex 001/2019) for the financial support. Authors thank D.Sc. Mariaugusta Ferreira Mota for the support in the spinning process and D.Sc. Bruno Alessandro Silva Guedes de Lima for AFM analysis.

Author Contributions Danyella Carolyna Soares dos Reis[1]: methodology, roles/writing—original draft.

Camila Rodrigues Borges Linhares[1]: methodology.

Rosiane Maria da Costa Farias[2]: methodology.

Deborah Santos Gomes[2]: methodology.

Gelmires de Araújo Neves[2]: methodology.

Jonas Dantas Batista[3]: methodology, roles/writing—original draft.

Paula Dechichi[4]: writing—review & editing.

Leticia de Souza Castro Filice[5]: project administration, writing—review & editing.

Romualdo Rodrigues Menezes[2]: supervision, funding acquisition, writing—review & editing.

Flaviana Soares Rocha[6]: project administration, funding acquisition, supervision, writing—review & editing.

Data Availability The authors confirm that the data supporting the findings of this study are available within the article.

Declarations

Conflict of interest The authors have no relevant financial or non-financial interests to disclose.

References

1. Hannouche D, Zaoui A, Zadegan F, Sedel L, Nizard R (2011) Thirty years of experience with alumina-on-alumina bearings in total hip arthroplasty. Int Orthop. https://doi.org/10.1007/s00264-010-1187-1
2. Schierano G et al (2015) An alumina toughened zirconia composite for dental implant application: In vivo animal results. Biomed Res Int. https://doi.org/10.1155/2015/157360
3. Piconi C, Porporati AA (2016) Bioinert ceramics: Zirconia and alumina. Handbook of Bioceramics and Biocomposites. https://doi.org/10.1007/978-3-319-12460-5_4
4. Karlsson M, Pålsgård E, Wilshaw PR, Di Silvio L (2003) Initial in vitro interaction of osteoblasts with nano-porous alumina. Biomaterials 24(18):3039–3046. https://doi.org/10.1016/S0142-9612(03)00146-7
5. Song Y, Ju Y, Song G, Morita Y (2013) In vitro proliferation and osteogenic differentiation of mesenchymal stem cells on nanoporous alumina. Int J Nanomedicine. https://doi.org/10.2147/IJN.S44885
6. Toloue EB, Karbasi S, Salehi H, Rafienia M (2019) Potential of an electrospun composite scaffold of poly (3-hydroxybutyrate)-chitosan/alumina nanowires in bone tissue engineering applications. Mater Sci Eng C. https://doi.org/10.1016/j.msec.2019.02.062
7. Gao C et al (2014) Current progress in bioactive ceramic scaffolds for bone repair and regeneration. Int J Mol Sci 15(3):4714–4732. https://doi.org/10.3390/ijms15034714
8. Popat KC et al (2005) Influence of nanoporous alumina membranes on long-term osteoblast response. Biomaterials. https://doi.org/10.1016/j.biomaterials.2004.11.026
9. Naji A, Harmand MF (1991) Cytocompatibility of two coating materials, amorphous alumina and silicon carbide, using human differentiated cell cultures. Biomaterials. https://doi.org/10.1016/0142-9612(91)90118-T
10. Leary Swan EE, Popat KC, Desai TA (2005) Peptide-immobilized nanoporous alumina membranes for enhanced osteoblast adhesion. Biomaterials 26(14):1969–1976. https://doi.org/10.1016/j.biomaterials.2004.07.001

11. Webster TJ, Siegel RW, Bizios R (1999) Osteoblast adhesion on nanophase ceramics. Biomaterials. https://doi.org/10.1016/S0142-9612(99)00020-4
12. Mussano F, Genova T, Serra FG, Carossa M, Munaron L, Carossa S (2018) Nano-pore size of alumina affects osteoblastic response. Int J Mol Sci. https://doi.org/10.3390/ijms19020528
13. Song Y, Ju Y, Morita Y, Song G (2013) Effect of the nanostructure of porous alumina on growth behavior of MG63 osteoblast-like cells. J Biosci Bioeng 116(4):509–515. https://doi.org/10.1016/j.jbiosc.2013.04.007
14. Popat KC, Chalvanichkul KI, Barnes GL, Latempa TJ, Grimes CA, Desai TA (2007) Osteogenic differentiation of marrow stromal cells cultured on nanoporous alumina surfaces. J Biomed Mater Res - Part A. https://doi.org/10.1002/jbm.a.31028
15. Dewle A, Pathak N, Rakshasmare P, Srivastava A (Feb.2020) Multifarious Fabrication Approaches of Producing Aligned Collagen Scaffolds for Tissue Engineering Applications. ACS Biomater Sci Eng 6(2):779–797. https://doi.org/10.1021/acsbiomaterials.9b01225
16. Lin W, Chen M, Qu T, Li J, Man Y (2020) Three-dimensional electrospun nanofibrous scaffolds for bone tissue engineering. J Biomed Mater Res Part B Appl Biomater. https://doi.org/10.1002/jbm.b.34479
17. Chen Y, Dong X, Shafiq M, Myles G, Radacsi N, Mo X (2022) Recent Advancements on Three-Dimensional Electrospun Nanofiber Scaffolds for Tissue Engineering. Adv Fiber Mater. https://doi.org/10.1007/s42765-022-00170-7
18. Medeiros ES, Glenn GM, Klamczynski AP, Orts WJ, Mattoso LHC (2009) Solution blow spinning: A new method to produce micro- and nanofibers from polymer solutions. J Appl Polym Sci. https://doi.org/10.1002/app.30275
19. Costa DL, Leite RS, Neves GA, de Santana LNL, Medeiros ES, Menezes RR (2016) Synthesis of TiO2 and ZnO nano and submicrometric fibers by solution blow spinning," Mater Lett, https://doi.org/10.1016/j.matlet.2016.07.073
20. Santos AMC, Mota MF, Leite RS, Neves GA, Medeiros ES, Menezes RR (2018) Solution blow spun titania nanofibers from solutions of high inorganic/organic precursor ratio. Ceram Int. https://doi.org/10.1016/j.ceramint.2017.10.096
21. Farias RMDC, Menezes RR, Oliveira JE, De Medeiros ES (2015) Production of submicrometric fibers of mullite by solution blow spinning (SBS). Mater Lett. https://doi.org/10.1016/j.matlet.2015.02.111
22. Medeiros ELG et al (2021) 3D nanofibrous bioactive glass scaffolds produced by one-step spinning process. Ceram Int. https://doi.org/10.1016/j.ceramint.2020.08.112
23. da Costa Farias RM et al. (2018) Solution blow spun spinel ferrite and highly porous silica nanofibers, Ceram Int, https://doi.org/10.1016/j.ceramint.2018.03.099
24. Batista JD, Zanetta-Barbosa D, Cardoso SV, Dechichi P, Rocha FS, Pagnoncelli RM (2014) Effect of low-level laser therapy on repair of the bone compromised by radiotherapy. Lasers Med Sci. https://doi.org/10.1007/s10103-014-1602-8
25. Wang J, Yu X (2010) Preparation, characterization and in vitro analysis of novel structured nanofibrous scaffolds for bone tissue engineering. Acta Biomater 6(8):3004–3012. https://doi.org/10.1016/j.actbio.2010.01.045
26. Mahapatra A, Mishra BG, Hota G (2013) Studies on electrospun alumina nanofibers for the removal of chromium(vi) and fluoride toxic ions from an aqueous system. Ind Eng Chem Res. https://doi.org/10.1021/ie301586j
27. Kim JH et al (2014) Characterization and application of electrospun alumina nanofibers. Nanoscale Res Lett 9(1):1–6. https://doi.org/10.1186/1556-276X-9-44
28. Panda PK, Ramakrishna S (2007) Electrospinning of alumina nanofibers using different precursors. J Mater Sci. https://doi.org/10.1007/s10853-007-1581-2
29. Medeiros ELG et al (2016) Porous Bioactive Nanofibers via Cryogenic Solution Blow Spinning and Their Formation into 3D Macroporous Scaffolds. ACS Biomater Sci Eng. https://doi.org/10.1021/acsbiomaterials.6b00072
30. Davoodi E, Zhianmanesh M, Montazerian H, Milani AS, Hoorfar M (2020) Nano-porous anodic alumina: fundamentals and applications in tissue engineering. J Mater Sci Mater Med. https://doi.org/10.1007/s10856-020-06398-2
31. Walpole AR, Briggs EP, Karlsson M, Pålsgård E, Wilshaw PR (2003) Nano-porous Alumina Coatings for Improved Bone Implant Interfaces. Materialwiss Werkstofftech. https://doi.org/10.1002/mawe.200300707
32. Masters KS, Anseth KS (2004) CELL-MATERIAL INTERACTIONS. Adv Chem Eng. https://doi.org/10.1016/S0065-2377(03)29002-5
33. Hing KA (2005) Bioceramic bone graft substitutes: Influence of porosity and chemistry. Int J Appl Ceram Technol. https://doi.org/10.1111/j.1744-7402.2005.02020.x
34. Li L, Kang W, Zhuang X, Shi J, Zhao Y, Cheng B (2015) A comparative study of alumina fibers prepared by electro-blown spinning (EBS) and solution blowing spinning (SBS). Mater Lett. https://doi.org/10.1016/j.matlet.2015.08.016
35. Li L, Kang W, Zhao Y, Li Y, Shi J, Cheng B (2015) Preparation of flexible ultra-fine Al2O3 fiber mats via the solution blowing method. Ceram Int. https://doi.org/10.1016/j.ceramint.2014.08.085
36. Alizadeh A et al (2019) Culture of dental pulp stem cells on nanoporous alumina substrates modified by carbon nanotubes. Int J Nanomedicine. https://doi.org/10.2147/IJN.S189730
37. Deligianni DD, Katsala N, Ladas S, Sotiropoulou D, Amedee J, Missirlis YF (2001) Effect of surface roughness of the titanium alloy Ti-6Al-4V on human bone marrow cell response and on protein adsorption. Biomaterials. https://doi.org/10.1016/S0142-9612(00)00274-X
38. Youn HS, Jyoti MA, Kwak KA, Seo HS, Lee BT, Song HY (2011) Enhanced osteoconduction and angiogenesis of a three dimensional continuously porous Al2O3 implant. Mater Sci Eng C. https://doi.org/10.1016/j.msec.2011.05.016
39. Pedimonte BJ et al (2014) Morphological zeta-potential variation of nanoporous anodic alumina layers and cell adherence. Acta Biomater. https://doi.org/10.1016/j.actbio.2013.09.023
40. Vandrovcová M, Bačáková L (2011) Adhesion, growth and differentiation of osteoblasts on surface-modified

materials developed for bone implants, Physiol Res https://doi.org/10.33549/physiolres.932045

41. Aramesh M, Cervenka J (2014) Surface modification of porous anodic alumina for medical and biological applications. Nanomedicine 438:439–467. https://www.researchgate.net/publication/278683237_Surface_Modification_of_Porous_Anodic_Alumina_for_Medical_and_Biological_Application
42. Wenzel RN (1949) Surface roughness and contact angle. J Phys Colloid Chem. https://doi.org/10.1021/j150474a015
43. Webster TJ, Siegel RW, Bizios R (1999) Design and evaluation of nanophase alumina for orthopaedic/dental applications. Nanostructured Mater. https://doi.org/10.1016/S0965-9773(99)00283-4
44. Minakov AV, Pryazhnikov MI, Simunin MM, Dobrosmyslov SS, Kuular AA, Molokeev MS, Volochaev MN, Khartov SV, Voronin AS (2022) Rheological properties of colloidal suspensions of alumina nanofibers. J Mol Liq. https://doi.org/10.1016/j.molliq.2022.120385
45. Serrano-Lotina A, Portela R, Baeza P, Alcolea-Rodriguez V, Villarroel M, Avila P (2023) Zeta potential as a tool for functional materials development. Catal Today. https://doi.org/10.1016/j.cattod.2022.08.004
46. Kosmulski M (2011) The pH-dependent surface charging and points of zero charge: V. Update J Colloid Interface Sci. https://doi.org/10.1016/j.jcis.2010.08.023
47. James RO, Parks GA (1982) Characterization of aqueous colloids by their electrical double-layer and intrinsic surface chemical properties. Surf Coll Sci. https://doi.org/10.1007/978-1-4613-3204-6_2
48. Tan F, Liu J, Song K, Liu M, Wang J (2018) Effect of surface charge on osteoblastic proliferation and differentiation on a poly(ethylene glycol)-diacrylate hydrogel. J Mater Sci. https://doi.org/10.1007/s10853-017-1558-8
49. Tan F, Liu J, Liu M, Wang J (2017) Charge density is more important than charge polarity in enhancing osteoblast-like cell attachment on poly(ethylene glycol)-diacrylate hydrogel. Mater Sci Eng C. https://doi.org/10.1016/j.msec.2017.03.051
50. Dames JE, Causton B, Bovell Y, Davy K, Sturt CS (1986) The migration of osteoblasts over substrata of discrete surface charge. Biomaterials. https://doi.org/10.1016/0142-9612(86)90109-2
51. Price RL, Gutwein LG, Kaledin L, Tepper F, Webster TJ (2003) Osteoblast function on nanophase alumina materials: Influence of chemistry, phase, and topography. J Biomed Mater Res - Part A 67(4):1284–1293. https://doi.org/10.1002/jbm.a.20011
52. Tran N, Webster TJ (2009) Nanotechnology for bone materials. Wiley Interdiscip Rev Nanomedicine Nanobiotechnology 1(3):336–351. https://doi.org/10.1002/wnan.23
53. Ni S, Li C, Ni S, Chen T, Webster TJ (2014) Understanding improved osteoblast behavior on select nanoporous anodic alumina. Int J Nanomedicine 9(1):3325–3334. https://doi.org/10.2147/IJN.S60346
54. Liu X, Lim JY, Donahue HJ, Dhurjati R, Mastro AM, Vogler EA (2007) Influence of substratum surface chemistry/energy and topography on the human fetal osteoblastic cell line hFOB 1.19: Phenotypic and genotypic responses observed in vitro, Biomaterials, https://doi.org/10.1016/j.biomaterials.2007.06.016
55. Anselme K, Ponche A, Bigerelle M (2010) Relative influence of surface topography and surface chemistry on cell response to bone implant materials Part 2 Biological aspects. Proc Inst Mech Eng Part H J Eng Med 224(12):1487–1507. https://doi.org/10.1243/09544119JEIM901